A general shape optimization method based on FFD approach with application to a high-speed train

ZHANG Ye, YANG GuoWei*, SUN ZhenXu&GUO DiLong
Key Laboratory for Mechanics in Fluid Solid Coupling Systems
Institute of Mechanics, Chinese Academy of Sciences
Beijing, China
Email: gwyang@imech.ac.cn

***Abstract*—A free form deformation parametric technique for high-speed trains is developed and 16 design variables are extracted to control the deformation of the streamlined nose shape. Combined with the proposed parametric technique, a multi-objective optimization design approach for aerodynamic head shape of the high-speed train based on Kriging surrogate model and the non-dominated sorting particle swarm optimization algorithm is proposed. The optimization results show that the free form deformation parametric technique can be well applied to the aerodynamic shape optimization of the high-speed train. After optimization the aerodynamic drag coefficient of the whole train and the lift coefficient of the tail car are reduced obviously. The parametric technique for high-speed trains and optimization approach developed in the present paper are simple yet efficient, and have important significance to the multi-objective engineering optimization design for high-speed trains.**

Keywords—free form deformation; particle swarm optimization; multi-objective; high speed trains

I. INTRODUCTION

Aerodynamic shape optimization design has made considerable progress during the past two decades with the development of computational fluid dynamics (CFD) and computer-aided design (CAD) techniques. General optimization methods can be divided into surrogate-based optimization [1-2] and gradient-based optimization [3-4]. One of the key problems that need to be solved for the two methods is to establish a shape parameterization technique which can control the deformation of the geometric shape effectively and satisfy the practical engineering constraints. Various parameterization techniques have been developed in the field of aircraft shape optimization design. Hicks and Henne [5] proposed a compact formulation for parameterization of airfoil sections, Sobieczky [6] introduced the PARSEC method for airfoil shape representation, Kulfan and Bussoletti [7] developed the Class function / Shape function Transformation (CST) parameterization technique, Sederberg [8] proposed free form deformation (FFD) method in field of computer graphics and it has been developed and applied into aircraft shape optimization.

In recent years, aerodynamic shape optimization design for high-speed trains has attracted more and more attention for the reason that aerodynamic problems appear more seriously as the running speed of high-speed train increases. The aerodynamic drag of high-speed trains can be up to 80% of the total drag at the speed of 300 km/h [9]. Resistance characteristics of the trains are directly related to the ability of energy saving and environmental protection [10]. Meanwhile, the wheel-track force is significantly reduced while excessive aerodynamic lift act on the train, which affects the operation safety. Parameterization techniques for aircraft cannot be applied to high-speed trains directly as the differences in appearances and constraint conditions. In the present paper, a FFD parameterization method for nose shape of high-speed train is developed and 16 design variables are extracted. Based on non-dominated sorting particle swarm optimization algorithm and Kriging model, a multi-objective surrogate-based optimization for high-speed trains is carried out. According to the presented method, Pareto optimal solutions are obtained. After that, aerodynamic performance of the optimized shape and the original shape of the high-speed train is comparatively analyzed.

II. FREE FORM DEFORMATION

The FFD technique allows the deformation of an object in a 2D or 3D space. It is based on the idea of embedding an object into a parallelepiped lattice of control points and transforming the object as the lattice deforms. The displacements of control points can be defined as the parameterization design variables. In addition to the global coordinate system, FFD also features a local coordinate system that records the relative position between different points, as shown in Fig.1. Every point’s local coordinate in the space enclosed by the parallelepiped lattice does not change in the process of deformation. The relationship between local coordinate (s,t,u) and global coordinate (x,y,z) is defined as follows:

$$\mathbf{X}(x,y,z)=\mathbf{X}_0+s\mathbf{S}+t\mathbf{T}+u\mathbf{U} \quad (1)$$

When control points are evenly distributed in the parallelepiped lattice, the (s,t,u) coordinates of X can easily be found using linear algebra:

$$\begin{cases} s = \dfrac{\mathbf{T}\times\mathbf{U}\cdot(\mathbf{X}-\mathbf{X}_0)}{\mathbf{T}\times\mathbf{U}\cdot\mathbf{S}} \\ t = \dfrac{\mathbf{S}\times\mathbf{U}\cdot(\mathbf{X}-\mathbf{X}_0)}{\mathbf{S}\times\mathbf{U}\cdot\mathbf{T}} \\ u = \dfrac{\mathbf{S}\times\mathbf{T}\cdot(\mathbf{X}-\mathbf{X}_0)}{\mathbf{S}\times\mathbf{T}\cdot\mathbf{U}} \end{cases} \quad (2)$$

Obviously, $0 \le s,t,u \le 1$.

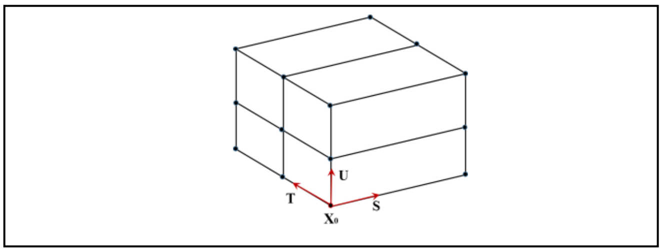

Fig. 1. *Local coordinate system*

The deformation function is usually defined by a trivariate tensor product Bernstein polynomial or B-splines basis [11]. In the present paper, the trivariate Bernstein polynomial is adopted. In summary, the deformed position $\mathbf{X}_{ffd}(s,t,u)$ of any arbitrary point with local coordinates (s,t,u) is given by

$$\mathbf{X}_{ffd}(s,t,u) = \sum_{i=0}^{l}\sum_{j=0}^{m}\sum_{k=0}^{n}\mathbf{P}_{i,j,k}B_{i,l}(s)B_{j,m}(t)B_{k,n}(u) \quad (3)$$

Where $\mathbf{P}_{i,j,k}$ is the i-th, j-th, k-th control point in the s, t, and u direction, and $B_{i,l}$, $B_{j,m}$, $B_{k,n}$ are l-degree, m-degree, n-degree Bernstein polynomials, respectively.

On account of the symmetry of nose shape of high-speed train, take the left half into a parallelepiped lattice with 18, 6, 5 control points in the x, y and z direction, respectively. Therefore, total number of the control points in the lattice is 540, as shown in Fig.2.

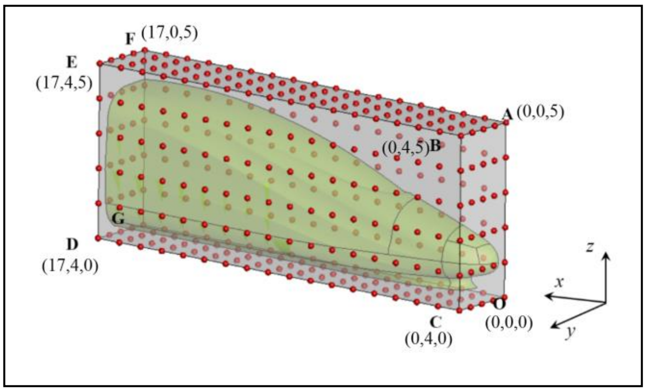

Fig. 2. *Parallelepiped lattice for a high-speed train*

Geometric constraints should be taken into consideration as the nose needs to be connected with other components of the high-speed train. Boundary DEFG is directly connected to the carriage, and the y and z coordinates of the control points on this plane should remain unchanged. Boundary OCDG is close to the track and the z coordinate variation of the control points should be limited in a small range so as not to intersect the track. Furthermore, because of the large number of control points, it is reasonable to choose the coordinates of the control points with obvious physical significance, which have great influence on the aerodynamic performance of the train, as the design variables. According to the engineering optimization experience, the following control points are selected as design variables, as shown in Table 1.

TABLE I. FFD DESIGN VARIABLES

Number	Design variable	Coordinate	Physical significance
1	(0,0,1)	x	Length of the nose
2	(0,0,1)	z	Height of the nose
3	(1,0,0)	x	Length of the cowcatcher
4	(1,1,0)	x	Length of the cowcatcher
5	(3,3,1)	z	Height of the diversion
6	(3,3,2)	z	Height of the diversion
7	(3,4,0)	y	Width of the bottom
8	(4,4,0)	y	Width of the bottom
9	(5,4,0)	y	Width of the bottom
10	(5,0,3)	z	Height of the cab
11	(6,0,3)	z	Height of the cab
12	(6,3,2)	z	Height of the cowcatcher
13	(9,4,2)	z	Height of the cowcatcher
14	(13,4,1)	y	Width of the nose
15	(13,4,2)	y	Width of the nose
16	(14,0,5)	z	Height of the roof

Fig.3 illustrates the corresponding deformation at different positions when changing the value of FFD design variables. It can be concluded that FFD parameterization technique can deform the target zone efficiently while it has less effect on other areas.

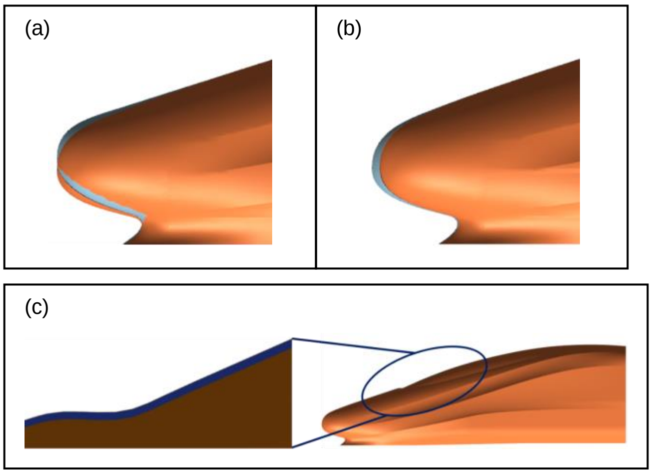

Fig. 3. *Parallelepiped lattice for a high-speed train,*(a)*Length of the nose*,(b)*Height of the nose*,(c)*Height of the cab*

III. NUMERICAL DETAIL

The train model adopted in the present paper is a full-scale Chinese Standard EMU train, which consists of a head car, a middle car and a tail car. The length of the head car and tail car are 26.5m while the length of the middle car is 25m. The height of the train is denoted by a characteristic length H of 3.50 m and the width of the car body is 3.38m. In consideration of the accessory parts' influence on aerodynamic performance of the high-speed train, windshields, the second bogie of the head car, bogies of the middle car and the first bogie of the tail car are included while the first bogie of the head car and the second bogie of the tail car are neglected for the convenience of deformation. The initial streamlined shape and the whole train model are shown in Fig.4 and Fig.5.

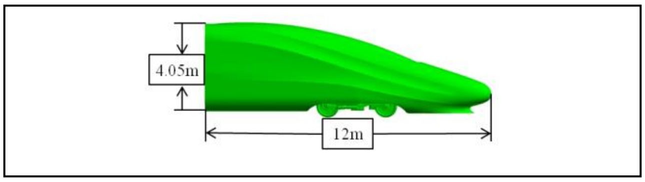

Fig. 4. *Initial streamlined head shape*

Fig. 5. *Train model*

In this paper, simulations were performed using the commercial software STAR-CCM+ which integrates the pre-processor, the CFD solver, and the post-processor into a package [12]. The STAR-CCM+ code provides various meshers and tools that can be used to generate quality meshes for complex geometries and different applications. In this study, a trimmed cell mesher was selected to generate the volume mesh and a prism layer mesher was selected to generate prismatic cell layers next to wall boundaries. The height of the first layer mesh was set to 0.8mm and the total thickness of the boundary layer was about 20mm, leading to values of y^+ between 30 and 100. Besides, local grid refinement is processed at the area of head car, bogies and windshields, as shown in Figure 6. The total number of volume cells was 21 million.

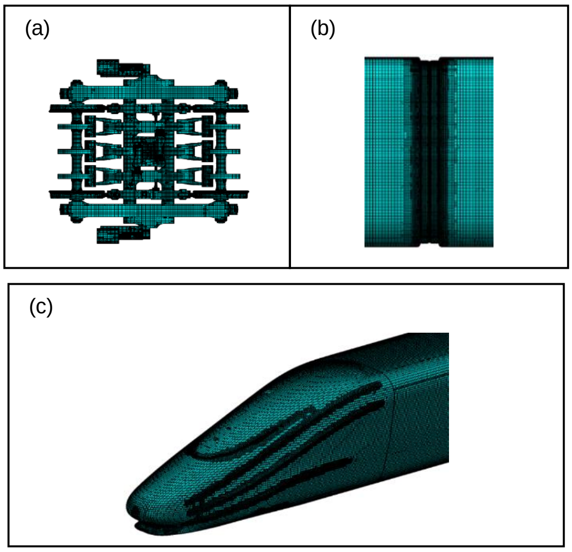

Fig. 6. *Surface mesh of different parts,* (a) *windshield,* (b) *bogie,*(c) *nose*

The computational domain is extended 30H beyond the nose of the head car and 60H from the tail car to the outlet. The height and width of the computational domain are 30H and 60H, respectively, as shown in Fig.7. By employing algorithm SIMPLE and a $k-\omega$ SST turbulent model, the steady incompressible Reynolds-averaged Navier-Stokes equations were used to solve the flow field. The inlet velocity was set to 300km/h (83.333m/s) and the ground was defined as moving wall with identical velocity as the air. The top wall and the side walls were set as slip walls.

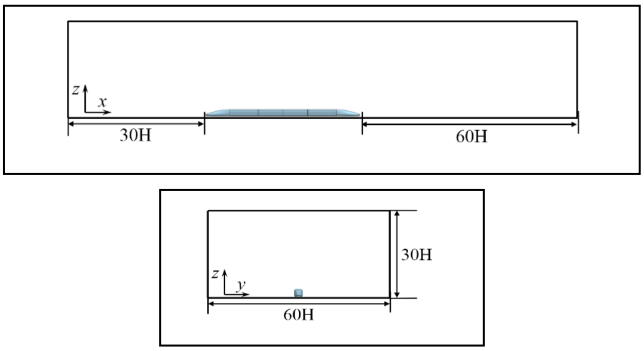

Fig. 7. *Computational domain*

IV. OPTIMIZATION METHODOLOGY

A. *Multi-objective particle swarm optimization*

Particle swarm optimization (PSO) is an evolutionary computation method which is originally proposed by Kennedy and Eberhart in 1995 [13]. The

PSO uses a simple mechanism that originally inspired by behavioral models of bird flocking to guide the particles to search for globally optimal solutions. The position of a particle represents a candidate solution to the optimization problem. Each particle searches for better positions in the search space by changing its velocity according to certain rules. During the evolutionary process, the velocity vector $V^i = \left(v_{i,1}, v_{i,2} \cdots v_{i,d}\right)$ and the position vector $X^i = \left(x_{i,1}, x_{i,2} \cdots x_{i,d}\right)$ of particle i on dimension d are updated as:

$$v_{i,j}\left(t+1\right) = wv_{i,j}\left(t\right) + c_1 r_1\left[p_{i,j} - x_{i,j}\left(t\right)\right] + c_2 r_2\left[p_{g,j} - x_{i,j}\left(t\right)\right] \quad (4)$$

$$x_{i,j}\left(t+1\right) = x_{i,j}\left(t\right) + v_{i,j}\left(t+1\right),\ j = 1, 2, \cdots d \quad (5)$$

Where w is the inertia weight, c_1 and c_2 are the acceleration coefficients, r_1 and r_2 are two distinct random values in [0, 1], p_i is the best previous position of the particle itself (*pbest*) and p_g denotes the best previous position of all particles of the swarm (*gbest*). The inertia weight w determines how much the current velocity of the particle is inherited and an appropriate value of w enables the balance between accelerating convergence speed and avoiding the local optima. During the past decades, different versions of PSO have been developed to solve multi-objective optimization problems. Coello et al [14] proposed an external file which saves every flight experience of particles for multi-objective optimization, Li [15] introduced the idea of non-dominated sorting, the niche count and crowding distance into PSO and developed the well-known Non-dominated Sorting Particle Swarm Optimization (NSPSO). Fig.8 shows multi-objective optimization results of four test functions using NSPSO. It can be concluded that it has a good performance in multi-objective optimization, therefore, the NSPSO is adopted in this paper for multi-objective optimization.

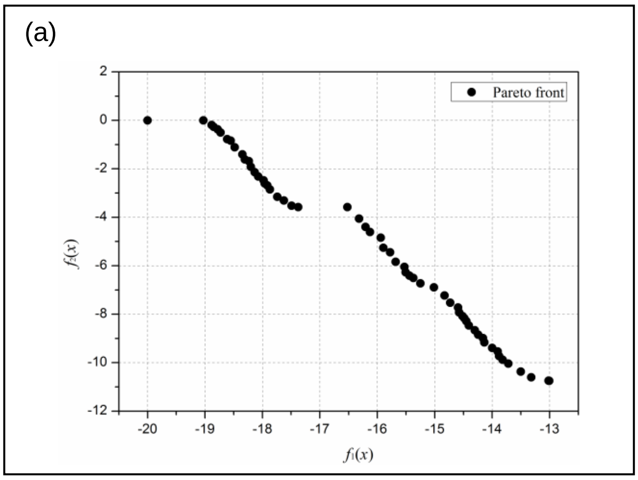

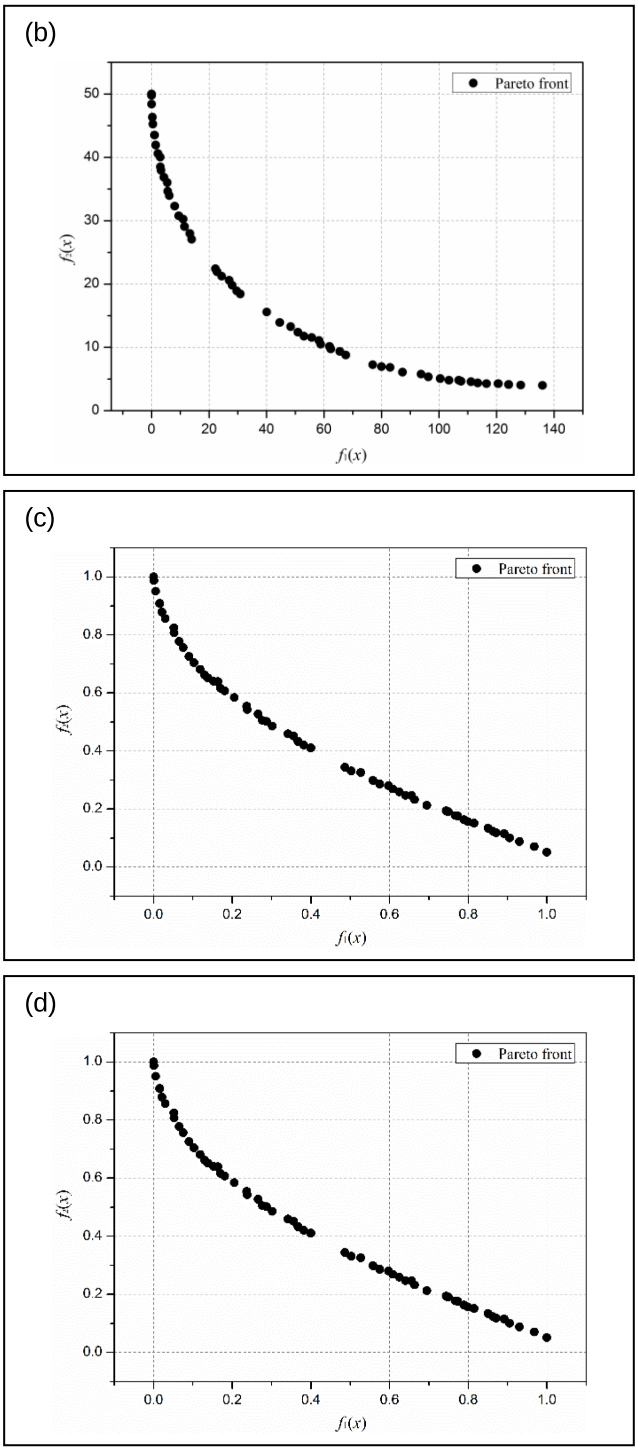

Fig. 8. *Numerical results of NSPSO,*(a) *Kursawe function,* (b) *Binh and Korn function,* (c) *ZDT function 1,* (d) *Schaffer function 1*

B. *Sample points and Kriging model*

In order to reduce the design cost, direct evaluations of the expensive high-fidelity simulation are replaced by the Kriging surrogate model [16] in this study. 40 sample points are generated using Latin Hypercube Sampling [17] technique according to the 16 FFD design variables. For all the sampling points, the aerodynamic drag coefficient of the whole train (C_d) and the lift coefficient of the tail car (C_l) are calculated, as shown in Table 2.

TABLE II. FFD TRAINING SAMPLE POINTS

Design variables	1	2	3	4	5	6	7	8	9	10	11	12	13	14	15	16	C_d	C_l
Range	(-60,30)	(-50,50)	(-50,30)	(-30,20)	(-25,20)	(-20,15)	(-30,30)	(-25,25)	(-25,25)	(-60,50)	(-50,40)	(-25,20)	(-25,20)	(-25,25)	(-25,25)	(-20,15)	--	--
1	0.37	0.06	0.69	0.33	0.88	0.29	0.89	0.22	0.46	0.28	0.79	0.28	0.80	0.56	0.43	0.76	0.285	0.0466
2	0.70	0.80	0.88	0.01	0.01	0.18	0.62	0.86	0.29	0.31	0.48	0.98	0.22	0.66	0.65	0.04	0.298	0.0513
3	0.70	0.64	0.43	0.57	0.75	0.49	0.29	0.62	0.60	0.88	0.62	0.68	0.63	0.19	0.85	0.20	0.291	0.0435
4	0.35	0.16	0.59	0.50	0.40	0.86	0.25	0.88	0.04	0.59	0.75	0.58	0.56	0.43	0.91	0.73	0.284	0.0415
5	0.12	0.02	0.38	0.60	0.20	0.59	0.53	0.99	0.98	0.91	0.90	0.26	0.18	0.92	0.53	0.59	0.294	0.0522
6	0.90	0.98	0.25	0.97	0.96	0.52	0.22	0.38	0.73	0.05	0.27	0.88	0.41	0.42	0.75	0.07	0.286	0.0481
7	0.48	0.69	0.87	0.64	0.99	0.82	0.98	0.57	0.26	0.93	0.01	0.76	0.61	0.75	0.50	0.45	0.289	0.0549
8	0.84	0.39	0.42	0.99	0.11	0.65	0.65	0.34	0.63	0.05	0.72	0.73	0.26	0.89	0.80	0.27	0.288	0.0480
9	0.95	0.48	0.46	0.73	0.32	0.03	0.59	0.93	0.20	0.72	0.97	0.67	0.50	0.78	0.04	0.88	0.291	0.0517
10	0.80	0.36	0.33	0.39	0.44	0.71	0.96	0.41	0.86	0.16	0.74	0.47	0.08	0.47	0.34	0.82	0.290	0.0496
11	0.53	0.30	0.71	0.27	0.51	0.01	0.91	0.32	0.35	0.75	0.99	0.31	0.45	0.32	0.13	0.01	0.289	0.0531
12	0.75	0.70	0.78	0.29	0.84	0.77	0.52	0.05	0.33	0.48	0.31	0.05	0.70	0.25	0.68	0.57	0.286	0.0415
13	0.27	0.66	0.92	0.91	0.58	0.84	0.74	0.46	0.68	0.24	0.34	0.33	0.04	0.70	0.46	0.63	0.279	0.0390
14	0.44	0.74	0.28	0.88	0.55	0.42	0.06	0.84	0.39	0.64	0.47	0.03	0.32	0.00	0.18	0.39	0.288	0.0472
15	0.90	0.22	0.50	0.49	0.93	0.62	0.42	0.79	0.56	0.21	0.07	0.15	0.53	0.39	0.96	0.42	0.295	0.0557
16	0.03	0.33	0.93	0.09	0.68	0.12	0.79	0.12	0.24	0.55	0.63	0.12	0.92	0.37	0.25	0.60	0.294	0.0528
17	0.01	0.91	0.12	0.37	0.13	0.24	0.02	0.54	0.89	0.79	0.43	0.21	0.74	0.84	0.72	0.50	0.284	0.0488
18	0.17	0.56	0.04	0.06	0.28	0.33	0.95	0.25	0.59	0.38	0.81	0.23	0.16	0.17	0.25	0.30	0.295	0.0517
19	0.99	0.95	0.74	0.46	0.46	0.95	0.86	0.65	0.91	0.13	0.54	0.08	0.24	0.12	0.11	0.79	0.292	0.0435
20	0.15	0.18	0.96	0.80	0.91	0.37	0.69	0.67	0.41	0.76	0.14	0.44	0.98	0.09	0.05	0.43	0.283	0.0416
21	0.39	0.60	0.56	0.60	0.35	0.32	0.04	0.59	0.18	0.55	0.22	0.65	0.39	0.13	0.94	0.16	0.288	0.0483
22	0.55	0.77	0.48	0.25	0.17	0.46	0.39	0.10	0.79	0.35	0.56	0.83	0.96	0.03	0.61	0.95	0.282	0.0461
23	0.67	0.26	0.67	0.15	0.35	0.55	0.50	0.69	0.52	0.66	0.38	0.93	0.13	0.85	0.17	0.53	0.287	0.0437
24	0.47	0.89	0.30	0.17	0.04	0.93	0.31	0.50	0.45	0.00	0.88	0.16	0.94	0.80	0.60	0.71	0.286	0.0505
25	0.97	0.85	0.99	0.83	0.48	0.88	0.33	0.75	0.66	0.34	0.09	0.00	0.77	0.53	0.64	0.33	0.292	0.0488
26	0.19	0.59	0.08	0.76	0.71	0.21	0.55	0.36	0.81	0.50	0.58	0.37	0.02	0.72	0.50	0.08	0.286	0.0531
27	0.32	0.46	0.18	0.53	0.41	0.64	0.12	0.14	0.01	0.45	0.93	0.79	0.59	0.22	0.28	0.11	0.289	0.0506
28	0.28	0.44	0.24	0.44	0.87	0.99	0.44	0.97	0.94	0.40	0.24	0.97	0.11	0.48	0.56	0.48	0.294	0.0481
29	0.59	0.54	0.77	0.70	0.56	0.06	0.81	0.49	0.16	0.85	0.83	0.61	0.71	0.74	0.77	0.70	0.294	0.0474
30	0.20	0.09	0.80	0.04	0.27	0.17	0.72	0.01	0.96	0.68	0.52	0.87	0.67	0.07	0.85	0.65	0.287	0.0479
31	0.52	0.24	0.22	0.85	0.08	0.91	0.26	0.91	0.50	0.26	0.16	0.53	0.28	0.97	0.39	0.25	0.293	0.0479
32	0.23	0.10	0.02	0.22	0.67	0.55	0.84	0.23	0.53	0.08	0.68	0.18	0.37	0.64	0.22	0.91	0.287	0.0494
33	0.06	0.51	0.84	0.69	0.82	0.69	0.76	0.15	0.13	0.62	0.87	0.55	0.87	0.52	0.98	0.35	0.285	0.0463
34	0.08	0.15	0.06	0.67	0.61	0.80	0.47	0.70	0.05	0.46	0.18	0.52	0.85	0.94	0.02	0.13	0.283	0.0362
35	0.80	0.40	0.36	0.94	0.24	0.38	0.64	0.44	0.70	0.96	0.41	0.50	0.89	0.58	0.88	0.99	0.286	0.0491
36	0.77	0.95	0.16	0.20	0.79	0.14	0.10	0.81	0.09	0.83	0.66	0.71	0.34	0.34	0.37	0.94	0.284	0.0454
37	0.62	0.81	0.61	0.32	0.05	0.43	0.13	0.05	0.31	0.18	0.04	0.82	0.82	0.61	0.79	0.21	0.291	0.0519
38	0.86	0.30	0.54	0.11	0.75	0.09	0.35	0.74	0.10	0.80	0.35	0.41	0.49	0.98	0.42	0.84	0.286	0.0422
39	0.65	0.83	0.15	0.82	0.20	0.27	0.15	0.18	0.77	0.11	0.29	0.91	0.43	0.29	0.31	0.87	0.292	0.0500
40	0.40	0.04	0.64	0.40	0.63	0.73	0.18	0.28	0.84	0.99	0.10	0.40	0.07	0.24	0.09	0.30	0.295	0.0524

The key problem for training Kriging model is to find the optimal values of parameters θ_i, i =1, 2, ⋯16. In the present paper, sample points 1 to 38 are used for the construction of Kriging model and the single-objective genetic algorithm [18] is chosen to obtain the optimal values of θ_i. Meanwhile, sample points 39 to 40 are used to test the prediction accuracy of the final Kriging model. Fig.9 illustrates the optimal values of θ_i, it can be seen that θ_2, θ_3, θ_4, θ_7 and θ_9 are significantly larger than the other, which suggests the corresponding design variables, height of the nose, length of the cowcatcher and width of the bottom have more effect on the aerodynamic performance of the high-speed train.

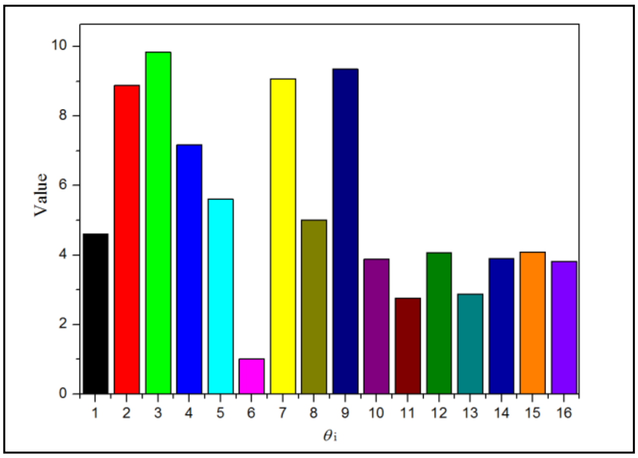

Fig. 9. *Optimal values of* θ_i.

Table 3 shows prediction accuracy of the Kriging model with the optimal θ_i. The prediction error for C_d is about 1% and within 5% for C_l. The test results indicate that optimal Kriging model performs well at predicting the aerodynamic drag and lift of the high-speed train.

TABLE III. PREDICTION ACCURACY OF KRIGING MODEL

Objective	Points	Actual Value	Predicted value	Error
C_d	39	0.292	0.289	**1.03%**
	40	0.295	0.292	**1.02%**
C_l	39	0.0500	0.0478	**4.40%**
	40	0.0524	0.0498	**4.96%**

V. RESULTS AND DISCUSSIONS

In the application to optimization design for high-speed trains, the aerodynamic drag coefficient and the lift coefficient of the tail car are treated as the optimization objectives, and the non-dominated sorting multi-objective particle swarm optimization is adopted to search for the Pareto front. The population of NSPSO is set to 100 and the number of generations is 1500, the optimal Kriging model is used to replace the CFD simulation during the optimization process. Fig.10 shows the Pareto solution of the C_d-C_l optimization based on FFD technique and NSPSO-Kriging approach. The result shows that a suitable Pareto front is obtained after iterations. For comparison, a specific individual is chosen as the design point, as the red star shows in Fig. 10.

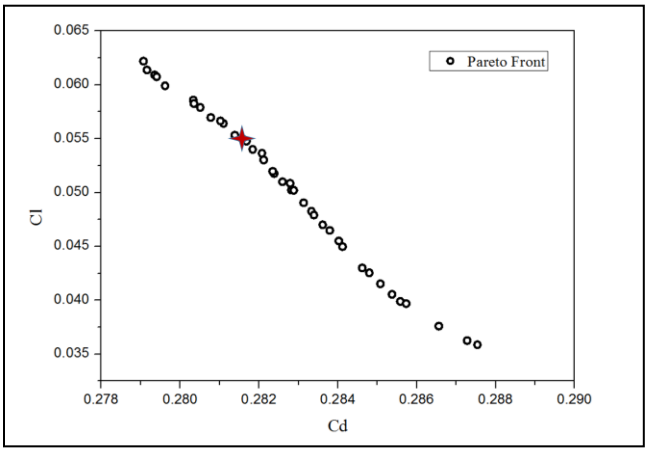

Fig. 10. *Pareto front.*

According to the optimization results, the values of FFD variables for the design point are listed in Table 4, then the final shape of the design point, namely the optimal shape, can be obtained. Fig.11 shows the comparison of the original shape and the optimal shape, where the orange one is the optimal shape and the green one is the original shape. It can be concluded from Table 4 and Fig.11 that the streamlined shape of the high-speed train deformed significantly after optimization at different positions. The length of the cowcatcher, the height of the cab, the width of the nose and the height of the roof decreased while the length and the height of the nose increased.

TABLE IV. FFD VARIABLES FOR THE DESIGN POINT

Design variable	1	2	3	4	5	6	7	8
Value	16.82	24.29	-46.21	-22.78	-6.60	1.79	-17.35	3.89
Design variable	9	10	11	12	13	14	15	16
Value	-15.85	45.61	-40.33	11.07	-16.32	-12.98	-15.23	-16.56

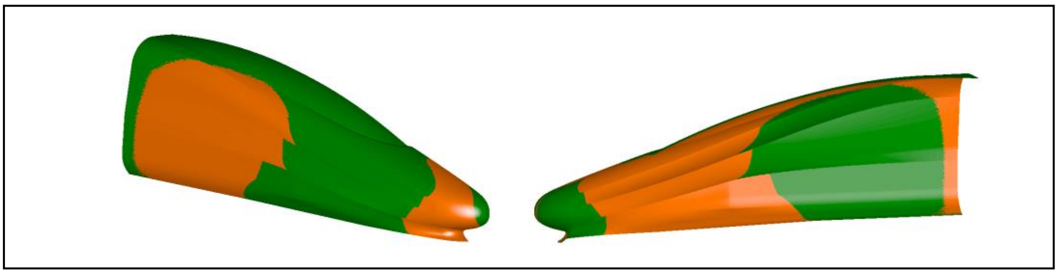

Fig. 11. *Comparison between the original shape and the optimal shape.(the orange is the optimal shape).*

Table 5 shows aerodynamic forces coefficients comparison between original and optimal shape. After optimization, the aerodynamic drag coefficient of the whole train is reduced by 3.13% and the aerodynamic lift coefficient of the tail car is reduced by 16.46%. Obviously, the optimal shape has better performance than the original one.

TABLE V. AERODYNAMIC FORCES COMPARISON

Objective	Original shape	Optimal shape	Reduction
C_d	0.2905	0.2814	3.13%
C_l	0.0662	0.0553	16.46%

Fig.12 illustrates the pressure contour comparison between the optimal shape and original shape, the surface pressure distribution of the original shape differs from the optimal shape in three areas: A1, A2 and A3. The surface pressure on the lower part of the nose decreased after optimization, as shown in A1. The shape of the nose side near the diversion was changed, resulting in a decrease in pressure in the area below the diversion, as shown in A2, and the width of the rear half of the nose increased, leading to an increase in the negative pressure in the A3 area.

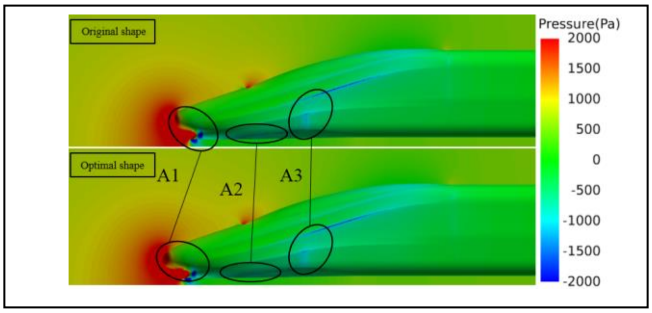

Fig. 12. *Pressure contour comparison between the optimal shape and original shape.*

In order to better understand the influence on aerodynamic lift of the tail car due to the change of nose shape of high-speed train, the iso-surface of the second invariant of the velocity gradient Q in the wake flow is shown in Figure 13. Four steady vortices V1, V2, V3 and V4 were developed along the surface of the streamline of the tail car, where V1 and V4 were more intense than the other two vortices. Meanwhile, there were some small steady vortices developed in the zone of cowcatcher, as shown in T1. After optimization, the strengths of V1, V3 and vortices in T1 were significantly reduced, as a result, the negative pressure of the optimal shape in the wake region was weaker than the original one, which could be helpful to reduce the aerodynamic lift of the tail car.

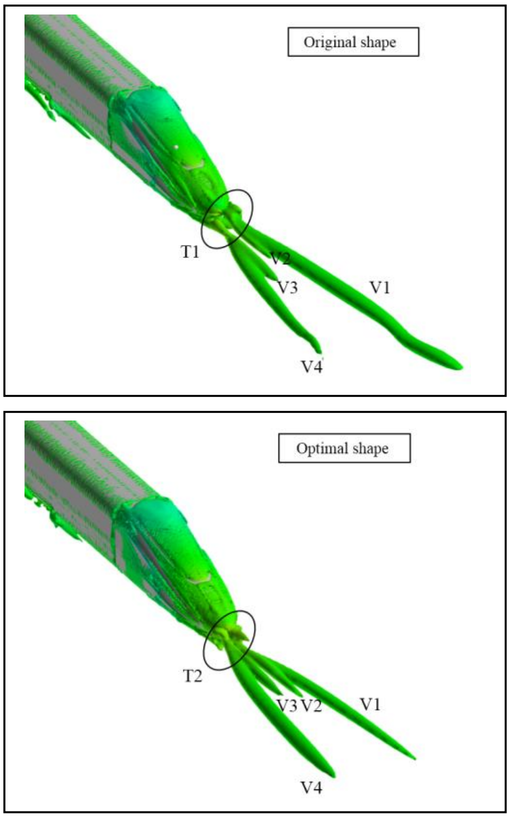

Fig. 13. *Transient Q iso-surface graphs around the tail car of original shape and optimal shape (Q=100).*

VI. CONCLUSIONS

In the present paper, a multi-objective optimization study was conducted based on the FFD parametric technique and NSPSO-Kriging approach to pursue the head shape of the high-speed train with lower aerodynamic drag and lift than the original one. Several conclusions have been obtained as follows:

1) The proposed FFD parametric technique for high-speed trains is simple yet practical. By adjusting the values of 16 design variables with specific physical significance, one can control the deformation of the nose shape efficiently.

2) The Kriging model with optimal values of parameters has a good performance at predicting the aerodynamic drag coefficient and lift coefficient.

3) The optimal shape shows better aerodynamic performance than the original one. After optimization, the aerodynamic drag of the whole train is reduced by 3.13% and the aerodynamic lift of the tail car is reduced by 16.46%. Surface pressure in certain areas of the nose and strengths of vortices in the wake region are both reduced for the optimal shape.

Acknowledgment

The Computing Facility for Computational Mechanics Institute of Mechanics at the Chinese Academy of Sciences is gratefully acknowledged.

References

[1] S., Koziel, L., Leifsson, "Surrogate-based aerodynamic shape optimization by variable-resolution models", AIAA journal, vol. 51, no.1, pp. 94-106, 2012.

[2] R. Datta, R. G. Regis, "A surrogate-assisted evolution strategy for constrained multiobjective optimization", Expert Systems with Applications, vol. 57, pp. 270-284, 2016.

[3] Antonio Baeza, Carlos Castro, Francisco Palacios, "2-D Euler Shape Design on Nonregular Flows Using Adjoint Rankine-Hugoniot Relations", AIAA Journal, vol. 47, no. 3, pp. 552-562, 2009.

[4] Francisco Palacios,Michael R. Colonno,Aniket C. Aranake, "Stanford University Unstructured (SU2): An open-source integrated computational environment for multi-physics simulation and design", AIAA Paper, pp. 287, 2013.

[5] Raymond M. Hicks, Preston A. Henne, "Wing Design by Numerical Optimization", Journal of Aircraft, vol. 15, no. 7, pp. 407-412, 1978.

[6] Helmut Sobieczky, "Parametric airfoils and wings", Springer, pp. 71-87,1999.

[7] Brenda M. Kulfan, John E. Bussoletti, "Fundamental parametric geometry representations for aircraft component shapes", pp.1-42, 2006.

[8] Thomas W. Sederberg, Scott R. Parry, "Free-form deformation of solid geometric models", SIGGRAPH Comput. Graph, vol. 20, no.4, pp. 151-160, 1986.

[9] G. Yang, D. Guo, S. Yao, C. Liu, "Aerodynamic design for China new high-speed trains", Science China Technological Sciences, vol. 55, no. 7, pp. 1923-1928, 2012.

[10] H. Q. Tian, "Formation mechanism of aerodynamic drag of high-speed train and some reduction measures", Journal of Central South University of Technology, vol.16, pp. 166-171, 2009.

[11] C. Schmutzler, A. Zimmermann, M. F. Zaeh, "Compensating Warpage of 3D Printed Parts Using Free-form Deformation", Procedia CIRP, vol. 41, pp. 1017-1022, 2016.

[12] Star CCM+ User Guide version 9.04, CD-adapco Corporation

[13] J. Kennedy, R. C. Eberhart, "Partical Swarm Optimization: Proceeding of the 1995 IEEE International Conference on Neural Network, Perth, Australia, pp.1942-1948, 1995.

[14] C. A. C. Coello, G. T. Pulido, M. S. Lechuga, "Handling multiple objectives with particle swarm optimization", IEEE Transactions on Evolutionary Computation, vol. 8, no. 3, pp. 256–279, 2004.

[15] X. Li, "A non-dominated sorting particle swarm optimizer for multi-objective optimization", Proceeding of Genetic and Evolutionary Computation GECCO 2003: Genetic and Evolutionary Computation Conference, Springer, pp.37–48, 2003.

[16] C. Noel, "The origins of Kriging", Math Geol, vol. 22, no. 3, pp. 239–252, 1990.

[17] V. J. Roshan, "Orthogonal-maximin Latin hypercubes designs", Stat Sin, vol. 18, no. 1, pp. 171–186, 2008.

[18] J.D. Bagley, "The behavior of adaptive system which employ genetic and correlation algorithm", PhD Thesis, University of Michigan, Michigan, USA, 1967.